Optical design trade study for the Wide Field Infrared Survey Telescope [WFIRST]

D. A. Content*[a], R. Goullioud[b], J. P. Lehan[c], J. E. Mentzell[a]
[a]NASA Goddard Space Flight Center, 8800 Greenbelt Rd, Greenbelt MD, USA 20771
[b]Jet Propulsion Laboratory, California Institute of Technology,
4800 Oak Grove Drive, Pasadena, CA USA 91109
[c]SGT, Inc., 7701 Greenbelt Road, Suite 400, Greenbelt MD, USA 20770

ABSTRACT

The Wide Field Infrared Survey Telescope (WFIRST) mission concept was ranked first in new space astrophysics mission by the Astro2010 Decadal Survey incorporating the Joint Dark Energy Mission (JDEM)-Omega payload concept and multiple science white papers. This mission is based on a space telescope at L2 studying exoplanets [via gravitational microlensing], probing dark energy, and surveying the near infrared sky. Since the release of NWNH, the WFIRST project has been working with the WFIRST science definition team (SDT) to refine mission and payload concepts. We present the driving requirements. The current interim reference mission point design, based on the use of a 1.3m unobscured aperture three mirror anastigmat form, with focal imaging and slitless spectroscopy science channels, is consistent with the requirements, requires no technology development, and out performs the JDEM-Omega design.

Keywords: Space astrophysics, exoplanet microlensing, Dark Energy, wide field imaging, three mirror anastigmat

1. INTRODUCTION

Our view of the universe has changed dramatically in recent years. We now know that most of the matter in the universe is invisible, and that the expansion of the universe is accelerating in an unexpected and unexplained way (dark energy). We now know there are many exoplanets, but have not fully determined their frequency or orbital distribution. Ground based experiments are ongoing and more are planned, but the atmosphere limits them: Atmospheric seeing and the limits of adaptive optics technology mean that wide field images are blurred. The near infrared spectrum is largely absorbed by water except for a few spectral windows. Observing transient phenomena (supernovae or exoplanet detections) requires calibration among multiple observatories which are hampered by weather and the circadian cycle. A space telescope with a wide field of view in the near infrared (NIR) spectrum can solve these challenges

Unlike prior decadal reviews, which chose among well-known candidate mission concepts, the Astro2010 Decadal survey (report: "New Worlds, New Horizons")[1] ranked the **Wide Field Infra-red Survey Telescope [WFIRST]** first in new space missions as a combination of the science and hardware concept from the Joint Dark Energy Mission[2,3] with the science agendas of the proposed Microlensing Planet Finder[4] and Near Infra-Red Sky Surveyor[5]. WFIRST will take precision images and spectra over thousands of square degrees, with very high image quality and stability greater than that of the Hubble Space Telescope (HST). A 50x wider field of view than Hubble's two-mirror telescope is required; our design uses a 1 square degree field unobscured three mirror anastigmat (TMA) design. Unobscured TMAs have been flown for earth-mapping telescopes and in ground telescopes, but not for an astrophysics space telescope. An enabling factor for the mission is the availability of near infrared (NIR) imaging array detectors which are can used to "tile" a large focal plane assembly.

This paper presents the initial design reference mission ("IDRM") for WFIRST, emphasizing the optical payload. As this design is, to a large extent, a derivative of the JDEM-Omega design[2,3], we refer to prior publications for its science and payload details. Another more current programmatic reference is the recently completed Interim Report[6] from the

*david.content@nasa.gov 301 286-7382; fax 1 301 286 0204

science definition team[7] working with the project office. Section 2 summarizes the changes in the science mission from those previously described for JDEM[2,3] and the resulting changes in requirements and emphasis. Section 3 describes the optical design trade space we explored and the reasons for the choices made in the current IDRM design. Section 4 describes the design and components. Section 5 explores stability that can be expected for the IDRM relative to the HST. We emphasize that, at this early stage, none of the design choices made should be assumed to be final or prescriptive.

2. REQUIREMENTS

All of the measurements require a large field of view in the NIR. Some also require visible to NIR spectroscopy as described below. The large field NIR imaging payload was a common thread among several proposals and white papers submitted to Astro2010. The large field and NIR combine two advantages of space observing over that obtainable from the ground, as should be the case to justify the larger cost: (1) the atmospheric seeing limit and the current and anticipated limits of extreme adaptive optics mean that image quality over large fields (we define very large field here as at least equal to 0.5° on a side, i.e. ≥0.25 square degrees), and (2) the accessibility of the near infrared region without water absorption. This means that the observing time for a 5 year mission (typically the longest planned mission for unserviced payloads that NASA plans) is oversubscribed. We mention first the new science and requirements and very briefly review the dark energy measurements[2,3,8,9] and ensuing requirements as they are largely unchanged in nature.

2.1 Exoplanet microlensing

Gravitational lensing provides a powerful way of detecting exoplanets, when a rare conjunction event occurs: If a background star and not only a foreground star but also a planet orbiting the foreground star align, the background star's light can be amplified through gravitational lensing. The time history of the flux, or light curve (see e.g.[10]) enables planet detection and can determine the planet orbital separation and the mass ratio of the planet to its host star.

By observing in the galactic bulge (the direction with the largest star density) with a 15 minute cadence, a large field imaging array can be expected to detect multiple planets even given the rarity of this alignment. The maximum probability of detection occurs much further from the star than detections made using multiple occultation method such as the Kepler mission[11]. The planets discovered could include Earth-like ones in habitable orbits as well as free (unbound) planets. This method is complementary to that of the Kepler and also to the radial velocity method[12]. Detailed follow-up observations, however, are unlikely.

The science objective in this area[6] is to "*complete the statistical census of planetary systems in the Galaxy, from habitable Earth-mass planets to free floating planets, including analogs to all of the planets in our Solar System except Mercury*."

The new requirements imposed on a JDEM-like observatory by adding this science include:

-Need for an enlarged field of regard to continuously monitor the galactic bulge for≥60 days up to twice a year

-Photometric accuracy in the imaging system to be able to see modest magnification events

-Increased emphasis on controlling in-field scattered light to minimize confusion in crowded fields.

2.2 IR surveys

WFIRST can be used as a powerful probe of the infrared sky. The decadal report says "*WFIRST will survey large areas of sky to address a broad range of Astro2010 science questions ranging from understanding the assembly of galaxies to the structure of the Milky Way*." It is expected that both the dark energy and exoplanet surveys will also provide a very rich data set that can be used, along with dedicated IR survey time, to address this science area. However the current understanding is that the requirements that flow down from this science influence the payload design mostly in the spectral bandpass and filter choices and not in the optical design itself.

2.3 Dark Energy

The accelerated expansion of the universe was discovered in 1998 through surveys of type 1a supernova [SN][13,14] which can be used as "standard candles" to independently measure both redshift and distance to their host galaxies. Three other measurement types have since added to our limited understanding: Baryon acoustic oscillations [BAO] where sound waves imprinted on the large scale cosmic structure have evolved into characteristic galaxy density fluctuations on known scales, acting as a standard ruler, Gravitational weak lensing [WL] measures the statistical correlation of galaxy shapes as a means of probing the intervening dark matter distribution. Redshift space distortion [RSD], uses the same wide galaxy redshift survey data as BAO, but emphasizes the redshift distribution more than the spatial distribution to help to constrain galaxy evolution, cosmic expansion, and the growth of cosmic structure.

In general the JDEM Omega design flowed from requirements based on this set of dark energy measurements. Some key requirements that drove that design are repeated here:

-At least 0.25 square degrees of imaging area and a selection of band pass filters with > $1m^2$ of aperture to allow wide sky imaging surveys to at least 25^{th} magnitude. (This requirement has consistently resulted in design studies for each of these science agendas in any combination in the choice of a three mirror anastigmat (TMA) telescope form.)

-Slitless spectroscopy of at least 0.5 square degrees, with multiple dispersion directions preferable to disentangle overlapping spectra of different object, at a resolving power sufficient to accurately centroid spectral H-alpha or other lines to determine the redshift of distant galaxies.

-Multiple fields of view and focal lengths to be able to rapidly obtain data for both the WL and BAO programs in parallel

-Filtered imaging and low resolving power spectroscopy to be able to identify supernovae, type them as 1a or not, and track the SN 1a light curves to determine both their redshift and absolute peak flux.

-Emphasis on photometric and point spread function stability for the SN and WL programs.

-Observatory must be cooled to $\leq$240K to not significantly emit thermal radiation in the 0.6-2.0 um band pass

2.4 Enveloping requirements

Overall the requirements dictate a large field of regard so that each target and sky survey area can be observed in enough depth and duration (for transient events, particularly the SN 1a and exoplanet microlensing events, each of which can last longer than one month). The image quality needed has been taken as a one micron diffraction limited system (71 nm rms), not including small amounts of pointing jitter, for the imaging, with some relaxation possible for the BAO slitless spectroscopy. Only the evolved expendable launch vehicle (EELV) [Atlas-5, Delta-IV heavy] and possibly the similar Falcon9 launch vehicles are capable of lifting this observatory to the 2^{nd} Lagrange point at which this field of regard and passive cooling of the observatory are practical.

Another driving requirement is the rule, to be developed quickly and at low risk, all technologies must be at TRL6 or approaching that with current funding. Given the funding levels, the optics design must require **no** technology development. This is in strong contrast to prior large space observatories. In particular we base the design on a single detector type nearly identical to the HgCdTe infrared 4-megapixel arrays used by JWST.

3. DESIGN TRADE SPACE

As we did with the "Probe" exercise[3], we first identified all of the potential design forms that could support these top level requirements. These subdivide into choices that have strong interactions with the science performance or not. Design choices that we considered with strong science performance interaction include:

1. Aperture size and type – obscured (oTMA) or unobscured (uTMA) telescope, diameter range 1.2-1.5m.

2. The number of science channels – single slitless spectrometer & imager, dual spectrometer & imager, or single channel with insertable dispersing element

3. Field area and focal length ratios (for multiple channel options) between imaging and spectroscopy

Design choices with weaker science interactions include:
1. Design form for each channel – focal or afocal; for afocal channels refractive or reflective cameras

2. Fixed or rotatable dispersion (for single spectrometer forms)

3. For an unobscured TMA there is a choice between a "Z" layout with large negative back focal distance, such that the intermediate focus is offset from but in between the primary and secondary, typically resulting in a focal plane high up near the secondary mirror; or a form with a longer focal distance and the instrument further back.

We explored each of these alternatives in an extensive design iteration phase. Previous designs included JDEM/IDECS (afocal, oTMA with dual refractive spectrometers), JDEM/Omega (focal, oTMA with reflective collimator for the spectrometers and dual refractive spectrometers), and the Probe A (afocal, uTMA with reflective imager and single spectrometer cameras). There was also a Probe A focal design[15] alternative showing that powered prisms (Feŕy-like) in a converging beam can be used for the dispersion range of interest for BAO and SN spectroscopy, depending on the spectral band pass, field of view, and dispersion required.

The final choice of the IDRM payload design was a systems optimization including many variables, including: optical performance margin, field of view and inter-channel field of view alignment, mass, volume, top level integration and test considerations, pupil imaging quality, and point spread function (PSF) quality.

4. INTERIM DESIGN REFERENCE MISSION PAYLOAD

The IDRM payload is a dual spectrometer focal, long form uTMA with a 1.3m aperture. We describe the design, the overall payload, and document basic performance in the following subsections.

4.1 IDRM description

The major change from JDEM-Omega is the switch to an unobscured telescope form. The advantages of this form for dark energy science have been pointed out before[16-18], but include improved MTF since the large central obscuration for stray light baffles (JDEM-Omega had a 50% linear obscuration) is not needed, improved sensitivity due to no loss of area, and increase in flexibility in design due to the aperture bias that more naturally allows beam clearance. One advantage of the uTMA over the three mirror system without an intermediate focus is the stray light reduction possible by the placement of a field stop at the intermediate focus, limiting stray light entering the instrument volume. Drawbacks of the unobscured form include larger overall telescope packaging volume, somewhat tighter alignment tolerances, and potentially more difficult mirror fabrication and alignment. We felt this last point is often overstated when improvements in mirror fabrication and alignment tooling are taken into account. For example, the Landsat data continuity mission/operational land imager (LDCM/OLI) instrument is an unobscured, wide field of view four mirror system, and has been reported as having no problems or delays during fabrication and alignment[19].

One drawback in the Omega design was that the rectangular spectroscopy channel fields of view were oriented so that the long axes were perpendicular to the long axis of the imaging channel. The standard Korsch[20] TMA has an annular corrected field of view which pushes the designer towards such a field layout. However sky tiling with multiple observations is less efficient with this field arrangement. We addressed this by discovering that the dual spectrometer option can work well if one uses both the focal prism form as well as a focal length reducing lens set (Shapley lens) subsequent to the focal prisms.

The design is performed in three basic stages. First, the "superfield" or enveloping field of all channels is considered, and an unfolded TMA is designed based on this field. By considering sky tiling constraints, we designed square field spectroscopy channels slightly larger in one dimension than the narrow imaging axis. This first stage fixes the design for the primary and secondary mirrors. Compared to an obscured telescope, the primary mirror must be longer radius of curvature to be not significantly more difficult in terms of fabrication based on aspheric slope and departure. The second stage of the design addresses the tertiary mirrors for each channel, which sets not only the tertiary mirror prescription but also the exit pupil location and imaging quality. Finally, the instrument components including prisms,

Shapley lenses, and filters are designed, along with fine guidance hardware as needed, and the folding and packaging to fit the entire observatory in the launch fairing.

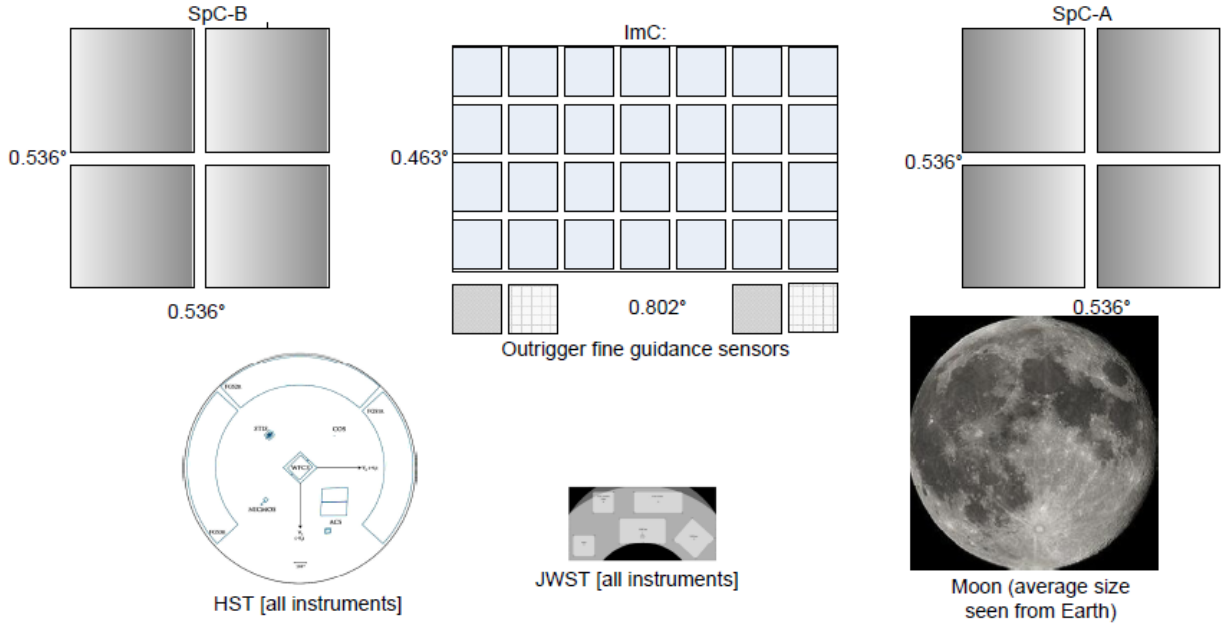

Fig. 1: Field of view diagram for the WFIRST interim design reference mission (top row). Each square is a 4Mpix HgCdTe array; different sizes denote differing pixel scales. SpCA & B are at right and left, ImC is centered in the field. Outrigger fine guidance channels are also in the ImC optical train and focal plane. An auxiliary guider (not shown) is available when the SN prism is selected via the filter wheel, placing a spectrum on the outrigger guidance sensors. Bottom Row: to-scale views of the JWST & HST, (all instrument) fields of view and the full Moon.

Figure 1 shows the field of view layout, along with views of the FOV layouts of JWST as planned and the current HST instrument complement FOV. In addition, we include the moon as seen from earth for an idea of scale on the sky. Each square in the figure is a 4Mpix HgCdTe NIR sensor chip assembly (SCA). However the pixel sizes are much coarser than those of the facility cameras on HST or JWST, as appropriate for a mission emphasizing wide surveys over pointed deep observations. Overall the imaging etendue (aperture area product with field of view area) is >10x that of HST/WFC3 or JWST/NIRCAM.

Compared to the JDEM-Omega concept, the total pixel count is preserved, but two NIR arrays are moved from each spectroscopy channel (SpC) to the imaging channel, such that the imaging mosaic increases from 6x4 to 7x4. The FOV loss with pixels in the spectrometers is compensated by a larger focal length ratio, increasing from roughly 2:1 in Omega to 2.5:1 here. The SpC field area is then as large as in Omega.

Figure 2 (top) shows a ray trace of the f/15.9 imaging instrument. The uTMA is folded after the aberrated intermediate focus. The tertiary mirror and subsequent fold mirrors are placed behind the primary mirror to be close to the mechanical load path from the telescope to the spacecraft, for maximum stability. A filter wheel is located just after the telescope exit pupil, which acts as the thermal/mechanical/optical interface between the telescope and imaging channel. The focal plane is located opposite the sun-viewing side so it can be placed close to a passive radiator. Similarly Fig. 2 (bottom) shows the two spectroscopy channel ray traces, the two channels being mirror images with dispersion directions opposed 80° on the sky to help disentangle overlapping spectra. Two folds surround the intermediate (Cassegrain-like) focus so that the ray bundle clears that of the imaging channel and is moved outside the ray bundle coming from the secondary mirror. The beam returning from the tertiary is folded away from the sun-illuminated side of the observatory. The spectrometer itself consists, as shown in Fig. 3, of a 3-prism group (zero deviation or direct vision

prism) and a 4-element Shapley lens. The beam entering the prism group is still f/15.9 and is reduced to f/6.9 by the Shapley lens. Each group's final surface has a mild conic, otherwise all instrument surfaces are spherical. All elements are vacuum-spaced for operation at ~170K. In the imaging channel one of the elements in the filter wheel is a low resolving power (R {2 pixel} ≥75) focal prism, used for spectroscopy of SN1a. The filter wheel elements, as decided by a consensus among the SDT, are described in Table 1.

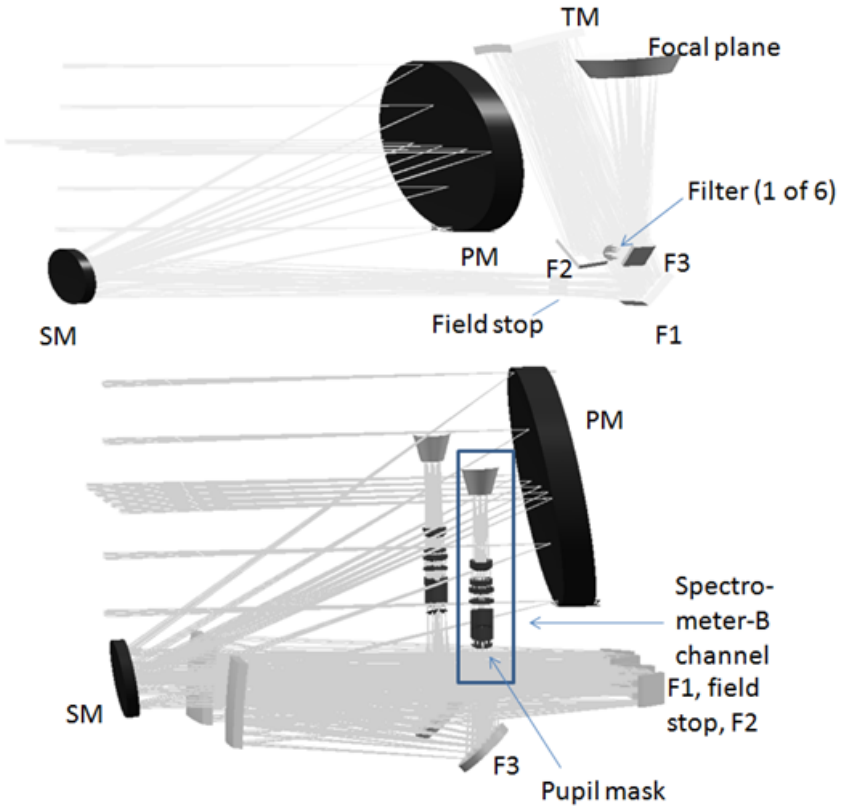

Fig. 2: Top: Ray trace of the Imaging Channel. ImC is an unobscured 1.3m three mirror anastigmat with a single fold between the intermediate focus and the tertiary, and two additional fold mirrors on either side of the exit pupil. The feed optics (non common telescope fold mirrors and tertiary mirror) and instrument (pupil mask, filter, and fold mirror) are packaged behind the primary mirror for stability. Bottom: Ray trace of the spectroscopy channels. SpC use two folds on either side of the intermediate focus and a third fold before the exit pupil to allow the instrument barrel to be located outside the telescope main barrel with the focal plane on the cold side of the observatory. The two channels A(far side) and B (near side) are mirror images. In both images the sun direction is towards the bottom of the page and the cold side of the observatory is at the top.

Table 1: List of filters and prisms for WFIRST IDRM1 instrument; wavelengths are in um.

name	min	max	center	type
F087	0.760	0.970	0.865	ImC filter
F111	0.970	1.240	1.105	ImC filter
F141	1.240	1.570	1.405	ImC filter
F178	1.570	2.000	1.785	ImC filter
W149	0.970	2.000	1.485	ImC filter
P130	0.6	2	1.3	ImC prism (R75)
SpC	1.114	2	1.557	SpC prism (R200)

4.2 Payload brief description

Overall the payload is designed with stray light control for an observatory which must observe most of the sky over its lifetime. The supernova measurements are made towards the galactic poles for minimal background. Conversely the exoplanet measurements are made looking at the galactic

central bulge with a high stars density. The IR survey looks both at high galactic latitudes along with a dedicated look in the galactic plane. The galaxy survey measurements (BAO, RSD, WL) will be initially done at high galactic latitudes, working closer to the galactic and ecliptic planes as time permits. Therefore we oriented the unobscured telescope so that the opening in the telescope tube between the PM and SM is facing away from the solar vector so that a full wall of ring baffles can be used to block any diffracted light. A large solar array/thermal shroud surrounds the optical and metering components so that no direct sunlight illuminates them for any field of regard.

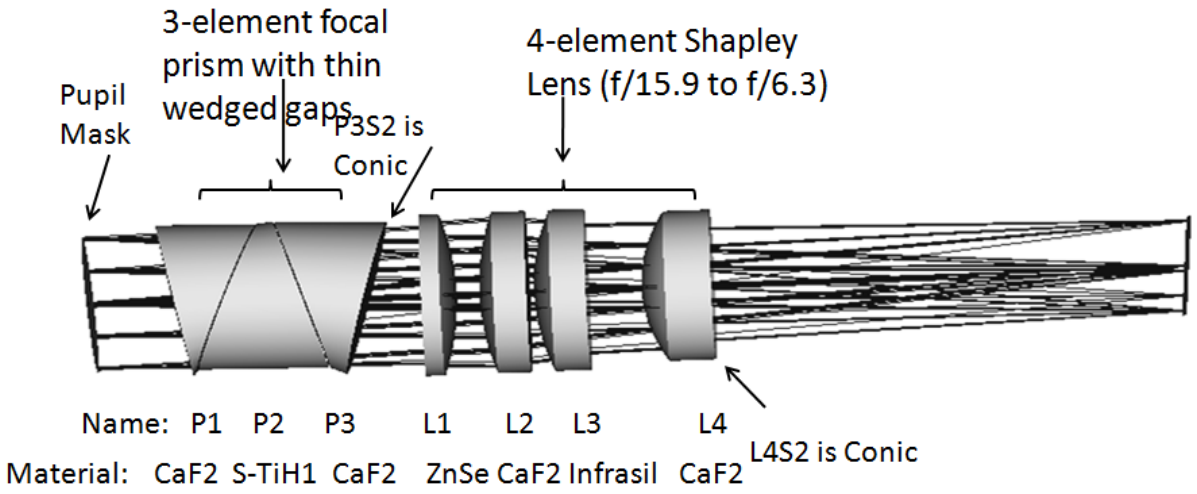

Fig. 3: Detail of spectroscopy channel, showing the prism and Shapley lens groups. Of 14 surfaces, 12 are spherical and 2 are weak conics. The prism is testable without the Shapley group, and the telescope is testable alone, or with the prism group as a f/15.9 system, or as a complete f/6.3 channel.

Figure 4 shows the observatory block diagram, including the telescope to instrument interfaces. The three tertiary mirrors are almost identical, as different apertures of the same parent conic mirror. All three instrument channel interfaces from the telescope are focal f/15.9 pupils of similar size and so can be tested using common equipment. Figure 5 is a CAD view of the observatory. This view shows the solar array/thermal shroud which keeps sunlight off the payload throughout its field of regard. The only deployable element is an aperture cover in front of the primary telescope tube; the on-orbit layout as shown fits in the family of launch vehicles mentioned previously.

4.3 Payload optical performance

Overall performance margins are improved relative to the JDEM-Omega design We set as a rule of thumb a minimum of a factor of two between the overall required wavefront allocation and that at the worst field-wavelength combination for a given channel. The ImC has a uniform error, ranging from 12 to 19nm over the field including the outrigger FGS fields and the science field, as shown in Fig. 6 in a field map at 1um wavelength. Rather than showing multiple field maps at different wavelengths to document the SpC design residual, we use a box plot for each wavelength in Fig 7 to show the quartiles, average, and outliers of the distribution at several wavelengths. Both channel designs have additional margin beyond the factor of 2 minimum. The effective area for each filter and prism mode is shown in Fig. 8, including models of mirror reflectivity, cold stop blockage, antireflection coatings, and detector quantum efficiency.

Overall this design achieves higher sensitivity, lower noise, and therefore up to twice as short an integration time to the same signal to noise level as compared to the JDEM-Omega design.

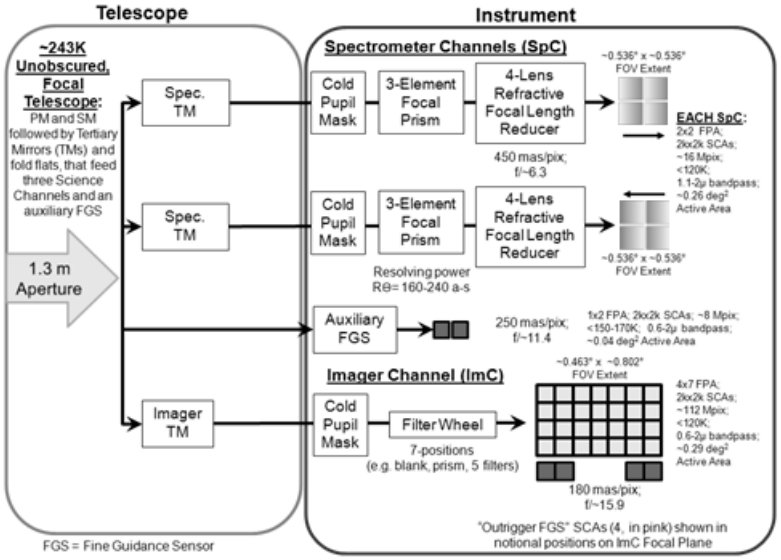

Fig. 4: Block diagram of the IDRM. This shows the interfaces, optical elements, and temperature zones of the payload.

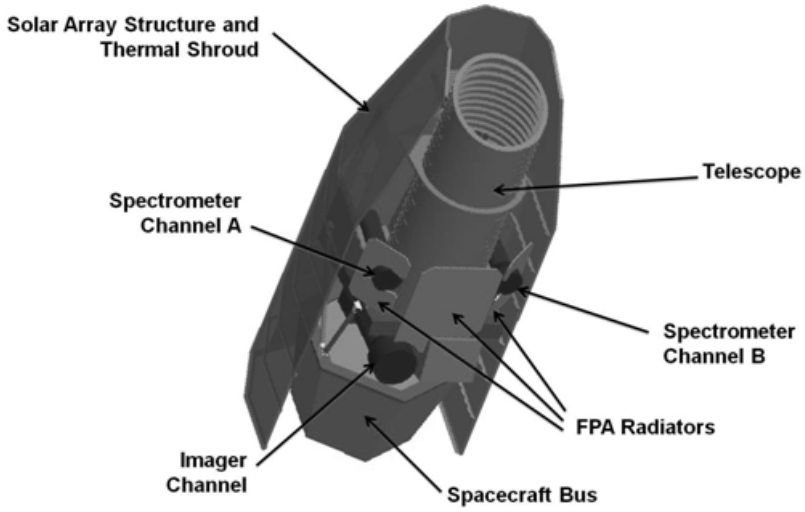

Fig. 5: Observatory CAD view, looking from the anti-Sun side. Focal planes and radiators are place facing anti-Sun and the Solar Array structure/thermal shroud shadows the payload to allow passive cooling. Each instrument channel mounts separately to the telescope structure.

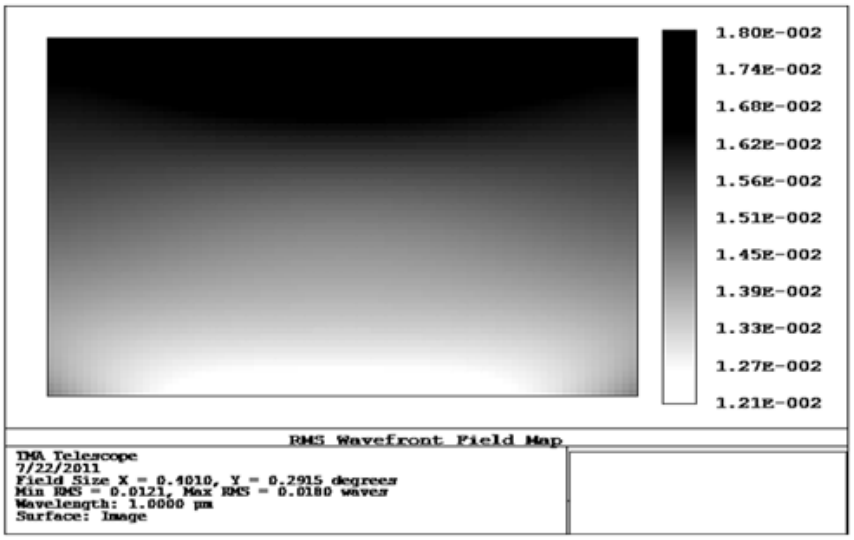

Fig. 6: Imaging Channel (ImC) residual error at 1um. Error is achromatic, uniform (12-18nm rms), and a small fraction of the 71nm rms total imaging budget.

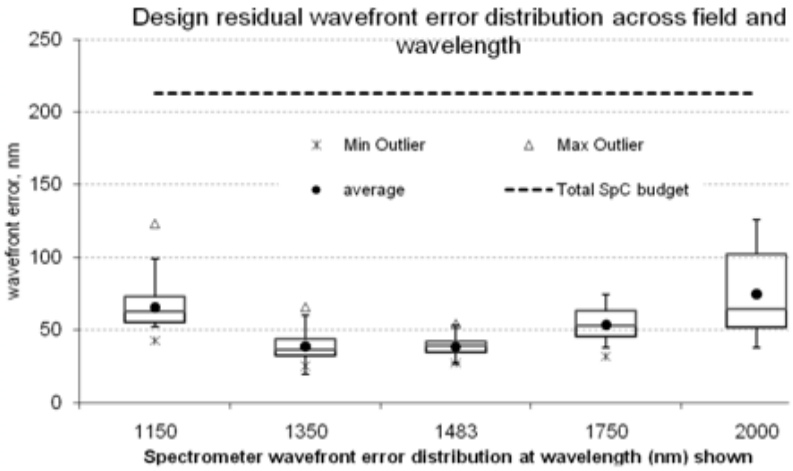

Fig. 7: Performance of SpC vs. wavelength. The distribution of errors across the field of view is shown as quartiles with outliers shown; robust margins against the total error budget are demonstrated.

5. STABILITY CONSIDERATIONS

One question that arises for the measurement which seems to require the most stringent system stability performance, weak gravitational lensing, is why we would expect our system to be more stable than the (much more expensive) Hubble space telescope (HST). We investigated the actual stability of the HST and compared it to our requirements as we understand them. We discuss first thermal, then pointing stability. As an example of the systematic error limits achieved to date with HST weak lensing observations we cite the COSMOS work[21] with an uncertainty in the systematic ellipticity of 0.01 when we expect to need < 0.001 or better for WFIRST.

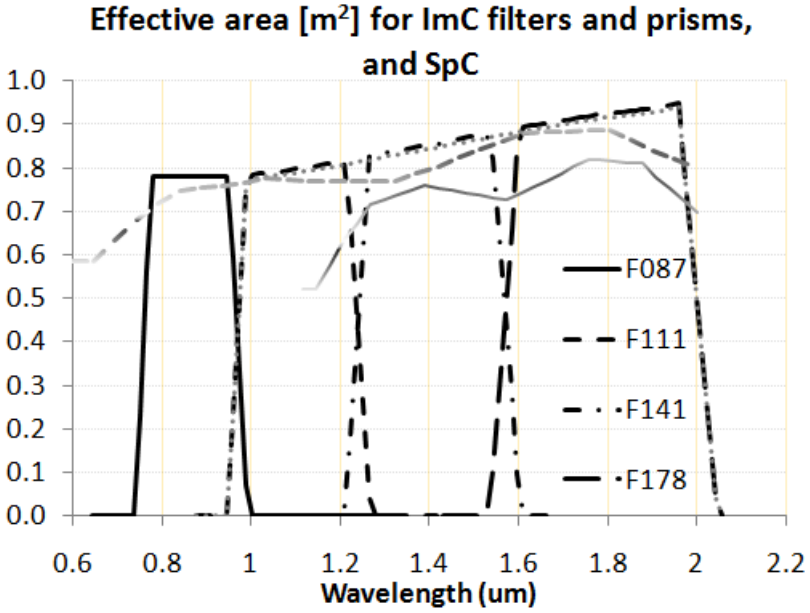

Fig. 8: Effective area (m^2) for each filter and prism mode; filters are as described in Table 1. Note the W149 very wide filter, used principally for exoplanet microlensing observations, overlaps at its blue edge with F111 and at its red edge with F178. The trend to greater efficiency at longer wavelengths is an effect of the combined detector QE and protected silver mirror coatings.

5.1 Thermal Stability

The HST is in low earth orbit, and has an operational requirement that when targets are obscured by the earth, HST remains 3 axis stabilized in that orbital attitude, so that earth light enters the aperture. Therefore, not only does the HST have earth thermal loading alongside the telescope during science integrations, but the thermal sink temperature of the aperture varies from cold deep space to night or daytime Earth temperatures. As documented in StSci reports[22-23], this behavior is now well understood empirically. The metering structure in HST metering the PM to the SM is 4.9m long, and has changes in axial gradient (the dominant term in the 'breathing' of HST focus) of 5° C. In addition, the effective CTE of the metering structure can be inferred from the empirical breathing model as follows: The coefficient of defocus is 0.81 um/° C where the motion is in linear units of movement of the SM. Including the metering distance, one infers and effective CTE of 0.165 ppm/ °C. This is about 4 times the material CTE of 0.045 ppm/ °C, and significantly larger than modern structural composites used at their design temperature. For WFRST each of these factors is less sensitive (CTE, metering distance, and secondary mirror magnification), reducing the defocus we can expect. As an example of what the combination of improved materials and the improvements that could be expected from a higher orbit that never puts earth in the aperture, we examined the case of the Chandra telescope[24]. Chandra has no worse than 0.2 degree gradients and has material with lower CTE. This is of order 50x or greater improvement in thermo-optical stability. This improvement suggests that a design of materials and thermal control similar to Chandra should suffice for thermal stability.

To be more specific, we analyzed the rms wavefront sensitivity of the {original design} HST and our IDRM to determine the defocus at the secondary (dS) required to create 5nm rms defocus wavefront error (w), which is of the order of the stability requirement. The results are similar, dw/dS =6.8 um for HST and 6.0 um for the WFIRST IDRM1 ImC. The defocus error one can expect can be calculated as w = dw/dS dT α S where dT is the change in gradient from PM to SM through the metering structure, α is the CTE (/°C), and S is the mirror separation. The results, shown in Table 2, show that defocus errors through thermal effects should be much lower on IDRM1 than are observed on HST even with significantly relaxed thermal control as compared to Chandra.

Table 2: Thermal stability tolerance comparison between HST and the WFIRST IDRM1 ImC, showing that we can expect significantly improved focus stability as compared to HST.

parameter	symbol	units	HST	IDRM1 ImC
wavefront defocus sensitivity	dw/dS	nm/um	6.8	6
mirror separation	S	mm	4900	2088
structure thermal expansion coefficient	α	ppm/°C	0.165	-0.09
Stability of thermal gradient	dT	C	±3	±1
length change	dS=S α dT	um	4.85	-0.38
defocus stability error	dw	nm	33.0	-2.3

5.2 Pointing Stability

The pointing performance of HST, on the other hand, is extremely good, typically no more than 4 milli arcseconds rms per axis and often better than that. HST has 3 fairly complex fine guidance cameras and large, well balanced reaction wheels as well as an observatory mass of ~11000 kg.

WFIRST pixels are much larger (e.g. 0.18" on ImC vs 0.04" on WF3) and we expect jitter and drift to be controlled to roughly 0.1 pixel; so 18 masec rms per axis should suffice even for WL. We would however download the pointing history as recorded by the FGS to allow ground reconstruction of the point spread function after jitter and drift are accounted for as part of the WL data reduction and analysis.

We expect to use closer to commercial wheels and less elaborate fine guidance systems for WFIRST, and work at observatory masses roughly in the 2000 kg range. Integrated modeling work done to date has indicated that we will need to:
-Mechanically (passively) isolate the reaction wheels
-Limit maximum wheel speed to (roughly) 2250 rpm to limit mechanical noise being input into the observatory
-Detune optical metering structure and telescope load path structure from the reaction wheel resonant frequencies
-(Possibly) passively isolate the payload from the spacecraft

However, we are unlikely to need active damping, either at the reaction wheel interface or the payload to spacecraft interface. Overall we feel that while challenging, achieving the pointing stability needed for WFIRST requires good engineering practice but again no new technology development.

6. SUMMARY

Overall this design performs well and is ready to proceed into detailed study and build phases. All of the required measurements can be accommodated. No technology funding is required. The interfaces are testable and standard; the margins appear robust. Integration and test planning appears straightforward and flexible. The much wider field of view of the TMA form and improved point spread function of the uTMA all appear to afford great survey discovery potential for both the nominal science measurements as well as the guest investigator program.

ACKNOWLEDGMENTS

We gratefully acknowledge that any work such as this is a product of the combined efforts of a large team. Particularly we want to thank the JDEM collaboration including the Science Coordination Group, the Interim Science Working Group, and the current WFIRST SDT. The engineering efforts are largely those of the project office, including N. Armani, N. Gehrels, K. Grady, C. E. Jackson, J. Kruk, M. Melton, C. Peddie, N. Rioux. We also thank past and present members of the optical design and engineering team, including M. Dittman, Q. Gong, J. M. Howard, G. Kuan, M. Quijada, M. Sholl, and M. Walthall.

REFERENCES

[1] Astro2010 final report: http://www.nap.edu/catalog.php?record_id=12951
[2] JDEM input to Astro2010: http://wfirst.gsfc.nasa.gov/science/astro2010_rfi/Astro2010_JDEM-Omega_RFI.pdf
[3] D. A. Content, M. G. Dittman, B. Firth, J. M. Howard, C. E. Jackson, J. P. Lehan, J. E. Mentzell, B. A. Pasquale and M. J. Sholl, "Joint Dark Energy Mission optical design studies", Proc. SPIE 7731, 77311D (2010); doi:10.1117/12.859144
[4] MPF input to Astro2010: http://arxiv.org/abs/0902.3000
[5] NIRSS input to Astro2010: http://wfirst.gsfc.nasa.gov/science/astro2010_rfi/Astro2010_NIRSS_RFI.pdf
[6] SDT interim report: http://wfirst.gsfc.nasa.gov/science/WFIRST_IDRM_Report_Final_signed_Rev1.pdf
[7] Science definition team for WFIRST membership: http://wfirst.gsfc.nasa.gov/science/sdt_membership.html
[8] Neil Gehrels, "The Joint Dark Energy Mission (JDEM) Omega," arXiv:1008.4936v1 [astro-ph.CO]
[9] Michael J. Sholl, Gary M. Bernstein, David A. Content, Michael G. Dittman, Joseph M. Howard, et al., "Observatory conceptual development for the Joint Dark Energy Mission", Proc. SPIE 7436, 743603 (2009); doi:10.1117/12.828116
[10] J.-P. Beaulieu, D. P. Bennett, P. Fouque, A. Williams, M. Dominik, et al., "Discovery of a cool planet of 5.5 Earth masses through gravitational microlensing," Nature Vol 439 (2006) doi:10.1038/nature04441
[11] Douglas A. Caldwell, Jeffrey E. Van Cleve, Jon M. Jenkins, Vic S. Argabright, Jeffery J. Kolodziejczak, et al., "Kepler instrument performance: an in-flight update", Proc. SPIE 7731, 773117 (2010); doi:10.1117/12.856638
[12] Stephane Udry, Nuno Santos, "Statistical Properties of Exoplanets," Ann. Rev. Astron. Astrophys. 2007. 45:397–439, doi: 10.1146/annurev.astro.45.051806.110529
[13] Riess, A. G., Filippenko, A. V. , Challis, P. , Clocchiatti, A., Diercks, A. et al., "Observational evidence from supernovae for an accelerating universe and a cosmological constant," A.J., 116, 1009 (1998).
[14] Perlmutter, S., Aldering, G., Goldhaber, G., Knop, R.A., Nugent, P. et al., "Measurements of Omega and Lambda from 42 high-redshift supernovae," Ap.J. 517, 565 (1999).
[15] Michael J. Sholl, David A. Content, Michael L. Lampton, John P. Lehan and Michael E. Levi, "Wide-field spectroscopy and imaging at two plate scales with a focal three mirror anastigmat", Proc. SPIE 7731, 77311F (2010); doi:10.1117/12.857762
[16] Gil Moretto, Maud P. Langlois and Marc Ferrari, "Suitable off-axis space-based telescope designs", Proc. SPIE 5487, 1111 (2004); doi:10.1117/12.548893
[17] Kuhn, J. R., Hawley, S. L., "Some Astronomical Performance Advantages of Off-Axis Telescopes," PASP 111 759 601-620 (1999).
[18] Michael L. Lampton, Michael J. Sholl and Michael E. Levi, "Off-axis telescopes for dark energy investigations", Proc. SPIE 7731, 77311G (2010); doi:10.1117/12.856500
[19] Michael G. Dittman and Brenda Firth, "OLI telescope post-alignment optical performance", Proc. SPIE 7807, 780705 (2010); doi:10.1117/12.860869
[20] Korsch, D., Appl. Opt. **11** #12 (1972), **16** #8 (1977), and **19** #21 (1980).
[21] Jason D. Rhodes, Richard J. Massey, Justin Albert , Nicholas Collins, Richard S. Ellis, et al., "The Stability of the Point-Spread Function of the Advanced Camera for Surveys on the Hubble Space Telescope and Implications for Weak Gravitational Lensing," Ap J. Supp., 172:203-218, (2007).
[22] Di Nino, D., Makidon, R. B., Lallo, M., Sahu, K., Sirianni, M., and Casertano, S, "HST Focus Variations with Temperature," Instrument Science Report ACS 2008-03, http://www.stsci.edu/hst/acs/documents/isrs/isr0803.pdf
[23] Colin Cox and Sami-Matias Niemi, "Evaluation of a temperature based HST Focus Model," Instrument Science Report TEL 2011-01, http://www.stsci.edu/institute/org/telescopes/Reports/ISR-TEL-2011-01.pdf
[24] Gary Matthews and Keith Havey, Jr., "Ten years of Chandra: reflecting back on engineering lessons learned during the design, fabrication, integration, test, and verification of NASA's great x-ray observatory", Proc. SPIE 7738, 77380Y (2010); doi:10.1117/12.858268